Simple finite-time sliding mode control approach for Jerk circuits: application on the synchronization of single Op-Amp-based Jerk circuits with PSpice verification

Nguazon Tekou [1], Nana Bonaventure [2], Tchitnga Robert [1] and Fomethe Anaclet [1]
1 Department of Physics, University of Dschang, Dschang, P.O.Box 67 Dschang, Cameroon
2 Department of Physics, University of Bamenda, Bamenda, P.O.Box 39 Bamenda, Cameroon

Abstract

In this paper, we extend the sliding mode idea to a class of third order Jerk system derived from a single Op-Amp-based jerk circuit. This method is achieved by the introduction of a single first order sliding equation. First, we have overcome the generally observed chattering phenomenon that occurs when the sliding mode control (SMC) method is applied to analyze the stability of coupled chaotic systems. Instead of an asymptotic convergence of the sliding equation corresponding to the SMC technique, we obtain rather a finite-time convergence and a linear sliding surface which is easy to implement experimentally. Applying the terminal sliding mode (TSM) method on the sliding equation leads directly to a convergence with fast terminal sliding mode (FTSM) method properties. Finally, several numerical simulation results have shown satisfactory control performances confirmed by PSpice simulations.

Keywords: Jerk circuit, chattering, synchronization, sliding mode, finite-time, control

Introduction

Linear and nonlinear sliding mode controls have been widely studied and applied on various systems [1], [2], [3], [4]. They are appreciated in robust control of systems for their inherent advantages in easy implementation, fast response, good transient performance, less sensitivity to parameter uncertainties and external disturbances [3] [5].

According to the type of sliding surfaces (linear or nonlinear), two kinds of sliding modes are found in the literature: the so-called sliding mode control (SMC) method dedicated to linear sliding surfaces and the later proposed terminal sliding mode (TSM) control technique used in finite-time stabilization for nonlinear sliding surfaces. The SMC method presents some drawbacks among which the fact that the system states can reach their equilibrium points only asymptotically [6], [7], and also, its implementation is marked by a pronounced chattering phenomenon [8]. The TSM method on the other hand may not be able to achieve quick convergence property when the initial states of systems are far away from their equilibrium points [6]. To overcome all the above mentioned limitations, the fast terminal sliding mode (FTSM) method has been elaborated, which combines the properties of both SMC and TSM methods, in addition to being fast [8], [9].

Using the sliding mode control method on a system implies to design an appropriate control law to be applied on the system error such that the sliding mode occurs on the linear sliding surface. Depending on the nature of systems, the design of such controllers can be very challenging with the usually required advanced mathematical developments. The authors of references [3] respectively [10] proposed a matrix approach for

the design of control method. On jerk systems, this approach is however suitable solely for those with simple and quadratic nonlinearities.

In the present paper, we aim at proposing a technique from the combination of existing methods for a more general solution that can be applied on any jerk system, even on those with piece wise nonlinearities. Thus, the principal objective of this paper is to address the synchronization of two jerk systems using the sliding mode control methods and techniques quoted in Refs. [3], [10], while the initial third order jerk equation has first been transformed into an implicit first order equation, the sliding equation [11], on which the sliding control methods have to be applied according to Ref. [7]. Furthermore, it is going to be observed that new insights on how to overcome the chattering phenomenon mentioned above will be derived from this approach.

The rest of the paper is organized as follows: In Section 2, after presenting the single op-amp-based jerk circuit, it sliding equation as well as the convergence conditions using the Lyapunov theorem are given. In Section 3, linear sliding manifold surfaces are used to synchronize two unidirectionally coupled systems. Section 4 deals with the fast finite-time synchronization of the two subsystems using two different nonlinear sliding manifold surfaces of sliding variables. This is followed by the comparison of different analyzed methods. In Section V experimental simulations are carried on for each of the three methods (SMC, TSM and FTSM) and the results compared to the numerical ones. The last section is devoted to the conclusion.

Model equations and convergence conditions

Model equations

The single op-amp-based jerk circuit is presented in Figure 1 it is made of two capacitors C_1 and C_2 one inductor L with internal resistance R, one operational amplifier assumed linear and one nonlinear element, the junction field-effect transistor J. According to Ref. [12] where all details on the application of electrical laws on that circuit are exposed, the dimensionless equations governing its dynamics is depicted by the following mathematical system:

$$\begin{cases} \dot{x} = h(y), \\ \dot{y} = \alpha(-z + h(y)), \\ \dot{z} = \beta(-x + y - \gamma z), \end{cases} \tag{1}$$

with $h(y) = -\min(1, y)$. Here x, y and z represent respectively the dimensionless voltages across the capacitors C_1 and C_2, as well as the current through the inductor. α, β and γ are the normalized parameters derived from the circuit components. After some mathematical manipulations, system (1) can be transformed into following corresponding jerk form:

$$\dddot{y} + \beta\gamma\ddot{y} + \alpha\beta\dot{y} = \alpha(\ddot{h} + \beta\gamma\dot{h} + \beta h). \tag{2}$$

As mentioned by the authors of reference [12], the system has a rich dynamics including chaotic oscillations for different combinations of its parameters. In the present work, following parameters' values are going to be considered: $\alpha = 0.0205$, $\beta = 0.362$ and $\gamma = 0.140$. The aim of this paragraph is to find the sliding equation of system (1). Inspired by the structure of the jerk equation (2) describing the same system, a new function g expressed in terms of the variable θ, $\dot{\theta}$ and $\ddot{\theta}$ of its first and second derivatives and can be defined as follows:

$$g(\ddot{\theta},\dot{\theta},\theta)=\ddot{\theta}+\beta\gamma\dot{\theta}+\alpha\beta\theta. \quad (3)$$

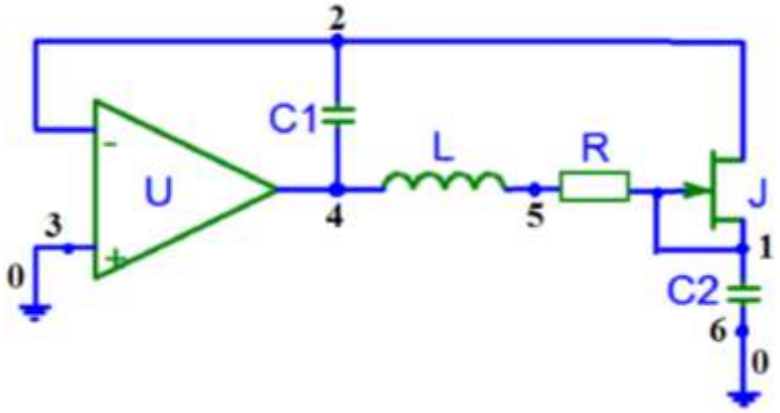

Figure 1: Single Op-Amp-based jerk circuit [12].

Exploiting the structure of equation (3), the former equation (2) can be reduced to an implicit first order form

$$\dot{g}=\alpha f+\alpha Ah, \quad (4)$$

Where $f=g(\ddot{h},\dot{h},h)$ and $A=\beta(1-\alpha)$. Equation (4) is the sliding equation of system (1) and g is its sliding variable [11].

In the rest of the paper, it is worth specifying that, for a given method, two approaches will be distinguishable: the usual approach where the system is a set of equations written in matrix form like in system (1), and the simple approach for which the system is transformed and written in the implicit form called the sliding equation (see equation (3)).

Convergence conditions

To proceed in a general way, consider the following differential equation:

$$\dot{X}=F(X) \quad \text{with} \quad F(0)=0,\ X\in R^n, \quad (5)$$

Where $F:D\to R^n$ is continuous on an opened neighborhood D of the origin. The equilibrium point X_0 of the system is (locally) finite-time stable if it is stable according to the Lyapunov criteria and finite-time convergent in a neighborhood $U\subseteq D$ [7]. In that case,

$$\lim_{T\to T(X_0)} X(t,X_0)=0. \quad (6)$$

It is important to note that, for any initial conditions $X_0\in U/\{0\}$, there is a settling time function $T(X_0):U/\{0\}\to(0,\infty)$ such that every solution $X(t,X_0)$ of the system represented by (5) is defined with $X(t,X_0)\in U/\{0\}$ for $t\in[0,T(X_0)]$ and satisfies $X(t,X_0)=0$ and (6), if $t\geq T(X_0)$. This assumes the finite-time convergence. Considering the nonlinear system described in (5) and assuming that there is a continuously differentiable function $V(X)$ defined in a neighborhood $(D\subset R^n)$ of the origin, it can therefore be deduced that

$$\dot{V}(X)+kV(X)+qV^a(X)\leq 0, \quad (7)$$

with $(k,q)>0,$ and $0<a<1$ being all real numbers. When $V(X)>0,$ on domain D then, the convergence time of the setting is

$$T(X_0) \le \frac{1}{k(1-a)} \ln\left(1+\frac{k}{q}V^{1-a}(X_0)\right). \quad (8)$$

It is obvious that the inequalities (7) and (8) include exponential as well as finite-time stability. This provides faster finite-time stability, compared to the TSM method [7].

Linear manifold

When two systems are coupled as drive and response, the output of the drive system is used to control the response system. If the controller satisfies certain conditions [2], the two systems will synchronize. In the following subsection, synchronization conditions for the present case will be developed.

Asymptotic SMC method: Usual approach

Consider a pair of nonlinear electronic oscillators described in the above sections, coupled in drive-response configuration as shown in equations (9) and (10).

$$\dot{X}_1 = MX_1 + F(X_1), \quad (9)$$

$$\dot{X}_2 = MX_2 + F(X_2) + u. \quad (10)$$

Here $X_i = (x_i, y_i, z_i)^T$ are the states variables of the system, $\begin{pmatrix} 0 & -1 & 0 \\ 0 & -\alpha & -\alpha \\ -\beta & \beta & -\gamma\beta \end{pmatrix}$ is the matrix of parameters, while $F(X_i) = \begin{pmatrix} 1 \\ \alpha \\ 0 \end{pmatrix} h(y_i)$ represents the nonlinear part of the system with $i=(1,2)$. The function h remains defined as in the previous section, namely $h(y_i) = -\min(1, y_i)$.

It is assumed that the synchronization is possible for any appropriate expression of the controller and the form of u needs to be determined. Then the stability of synchronization manifold is decided by the asymptotic behavior of $X = X_2 - X_1$ which obeys the following variational equation:

$$\dot{X} = MX + F(X) + u. \quad (11)$$

Now, let the controller u be designed using the SMC method. Otherwise, the synchronization error $X = X_2 - X_1$ will tend asymptotically to the equilibrium point $X_0 = (0,0,0)^T$. To achieve the SMC synchronization, the controller u is chosen such that

$$u = -F(X) + BV, \quad (12)$$

where B is a constant vector selected to make the product MB controllable; v (still to be determined) is a part of the controller u [2]. Next, the sliding surface s is determined to verify the following conditions:

$$s(X) = CX^T = 0, \tag{13}$$

and

$$\dot{s}(X) = C\left[MX + Bv\right] = 0. \tag{14}$$

The row vector C has to be determined to fulfill the condition $CB \neq 0$. To have the sliding condition satisfied so that the sliding motion can occur, let a first order sliding surface be defined as (15):

$$\dot{s} = -q \cdot \text{sign}(s) - ks, \tag{15}$$

with the gains $(q,k) > (0,0)$. Now, combining equation (25) and the Lyapunov function

$$V = \frac{1}{2}s^2, \tag{16}$$

leads to equation (17) that verifies the Lyapunov property:

$$\dot{V} = -2kV - q\sqrt{|2V|}. \tag{17}$$

Hence, the problem at this stage is to select the row vector C such that the matrix system of the controlled dynamics

$$M_C = \left[Id - B(CB)^{-1}C\right]M, \tag{18}$$

must satisfy the Hurwitz criterion. Yet if the Hurwitz criterion is satisfied then the controlled errors' system is globally asymptotically stable. From equations (14) and (15), the unknown part of the controller can be obtained as:

$$v(t) = -(CB)^{-1}\left[C(kId + M)X + q \cdot \text{sign}(s)\right], \tag{19}$$

where Id is the identity matrix. By giving arbitrary values to the constant vector B then applying the Hurwitz stability criterion on the characteristic polynomial equation from (18), the values of the row vector C can be obtained. In addition, the arbitrary choice of k and q enables computation of (19) which is then used to plot the results presented in $V = \frac{1}{2}s^2,$ Figure 2.

The initial conditions used to compute numerical results are $x_1 = 0.1$, $y_1 = -5 \cdot 10^{-7}$, $z_1 = 1$ for the drive, and $x_2 = 2$, $y_2 = -3 \cdot 10^{-4}$, $z_2 = 4$ for the slave systems respectively. The values of the controller parameters are worth $k = 4$; $q = 10^{-1}$; $B = \begin{pmatrix} 1 \\ 1 \\ 1 \end{pmatrix}$; $C = \begin{pmatrix} -5 & 20 & 0.23 \end{pmatrix}$. As predicted in Refs [6] and [8], results on Figure 2 are marked by the chattering phenomenon which induces the oscillation of error variables as revealed by the different zooms. It shows also that the precision achieved when the studied system converges asymptotically to the equilibrium point is of order of magnitude 10^{-3} .

In this approach some parameter values of the controller are given arbitrarily just to simplify the size of its computation which is still relatively large. This is why in the next approach developed in the following

section, only the sliding equation is going to be used, which has in the present case the direct consequence of transforming SMC into TSM method, even though the linear manifold is still used.

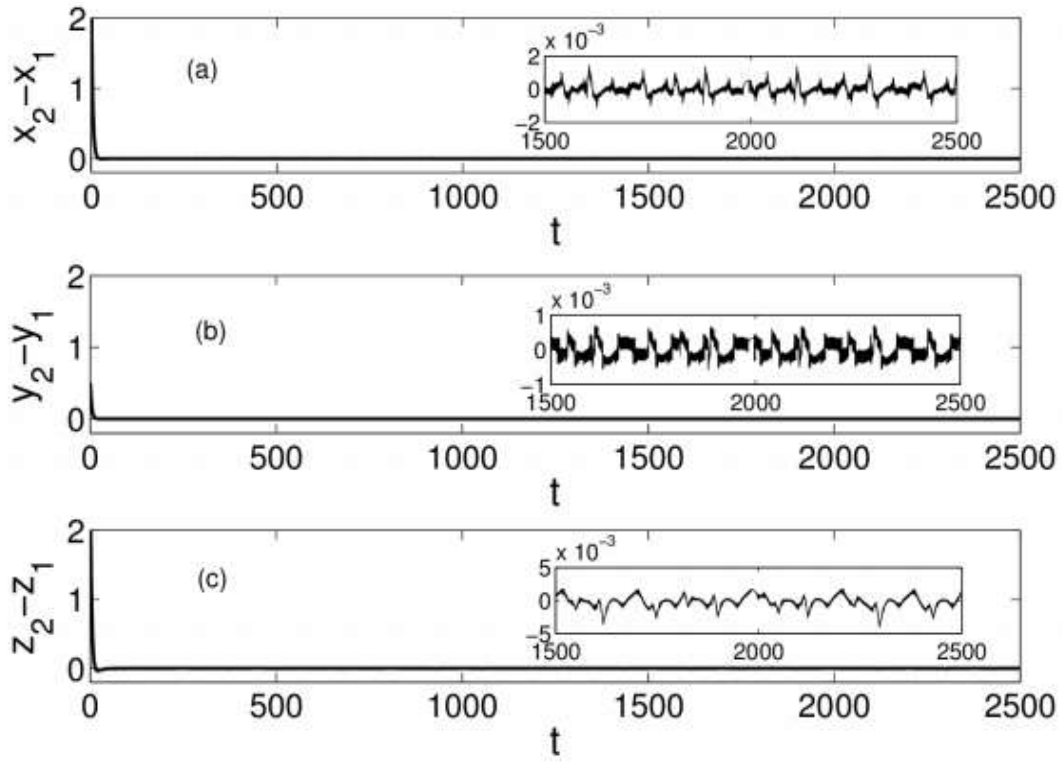

Figure 2: Synchronization error variable X versus dimensionless time t. Graphs a), b) and c) show error on x, y and, z variables respectively. Zooms inside the boxes underline the occurrence of chattering phenomenon that proceeds from the use of SMC techniques.

Asymptotic SMC method: Simple Approach

Contrary to the usual approach, the simple approach will give the SMC a convergence in finite time. In general, the finite-time convergence with respect to the sliding mode is obtained solely by a nonlinear surface manifold, which is called the TSM method. Yet, with the simple approach and a linear surface manifold, the following development will show that finite time can be achieved, although one is still dealing with the SMC method. It should be noted that the results obtained in this section offer the same advantages as the TSM method.

Instead of using the system of state equations (1) to achieve synchronization with SMC method as previously, let the sliding variable equation (4) be used, where the linear sliding surface is a function of the sliding variable. Consider two sliding equations

$$\dot{g}_1 = \alpha f_1 + \alpha A h_1 \tag{20}$$

$$\dot{g}_2 = \alpha f_2 + \alpha A h_2 + u \tag{21}$$

for the drive and response systems respectively, corresponding to (9) and (10). Then the sliding equation of errors is given by:

$$\dot{g} = \alpha f + \alpha A h + u, \tag{22}$$

with $g = g_2 - g_1$, $f = f_2 - f_1$, $h = h_2 - h_1$, and the sliding controller defined as

$$u = -\alpha f - Ah - qsgn(g) - kg. \tag{23}$$

Following the same procedure used in matrix form [2] the sliding manifold is defined as

$$s = Cg. \tag{24}$$

A convenient mathematical manipulation of equations (16), (22) and (24) leads to obtain the Lyapunov stabilization criteria

$$\dot{V}(g) + kV(g) + q\sqrt{2V(g)} = 0. \tag{25}$$

When the error system tends to the equilibrium point X_0, equations (7) and (25) show that the stabilization is no more asymptotic but finite-time with a synchronization time given by the following relation:

$$T(g_0) = \frac{2}{k}\ln\left(1 + \frac{\alpha}{q}\sqrt{V(g_0)}\right). \tag{26}$$

With arbitrarily chosen values of $k = 2$ and $q = 0.1$, the controller of (23) enables to obtain the curves of Figure 3.

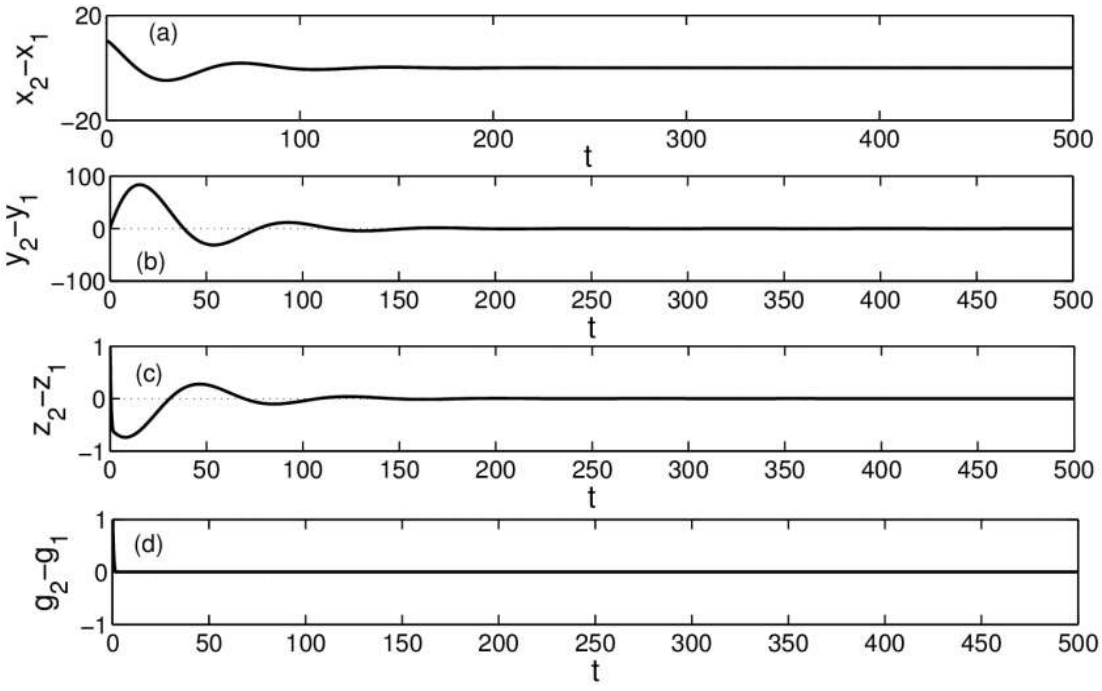

Figure 3: Synchronization error variable X versus dimensionless time t when implicit variable g is used. a), b), c) and, d) present the result with linear sliding surface. Graphs from top to bottom show in each column, error on x, y and, z error variables and the sliding variable g.

As it will be seen later on a comparative graph in section 4 of this paper, the curves of Figure 6 (red color) do almost not suffer anymore from chattering phenomenon. Furthermore, with precision between 10^{-8} and 10^{-5}, the error variables are far from the equilibrium point as well as the following initial conditions are also

chosen far from zero [6]. The initial conditions considered in the numerical simulations are $x_1 = 0.1$, $y_1 = -5 \cdot 10^{-7}$, $z_1 = -1$ for the master drive, and $x_2 = 10$, $y_2 = 2$, $z_2 = 1 \cdot 10^{-4}$ for the response systems respectively.

The SMC method applied on the states errors' system shows an asymptotic stability. Its application on the sliding equation provides the finite-time stability which improves the errors' system performance to high-precision and finite-time convergence to the equilibrium point [7]. Now that it has been proven how easy it is to use sliding equations instead of matrix form of states equations for synchronization, a nonlinear sliding manifold surface is going to be used for better performance stated by the authors of Ref. [13].

Nonlinear manifold

Finite-time method: Simple Approach

In the nonlinear manifold surface, there are two methods: the TSM and the FTSM. This later, thanks to its nonlinear manifold surface of second order, was designed to solve the problem of distance from the initial conditions that limits the TSM. However, with the present simple approach and a nonlinear surface, the following development will show that a nonlinear manifold surface of second order decreases the convergence time contrary to what is customary. Indeed, here, a nonlinear manifold surface (usually used for the TSM) is sufficient to have a quick convergence time with the advantages of the FTSM. The usual nonlinear manifold surface of both TSM and FTSM control methods satisfies the Lyapunov criteria of stability [6, 7, 8] and is given respectively by:

$$s = \dot{X} + b|X|^{a} \, sign(X) = 0, \tag{27}$$

and

$$s = \dot{X} + \ell X + b|X|^{a} \, sign(X) = 0. \tag{28}$$

Here: $(\ell, b) > (0,0)$, $a = \frac{p}{m}$ is an irreducible fraction with $a \in (0,1)$, m>p>0 are odd integers, and x is the state variable of the system. These nonlinear sliding surfaces are used in the present case but with an additional condition that m must be odd.

Following the drive-response formalism, equation (22) is considered again with a different form of the controller given by:

$$u = -\alpha f - \alpha A h - Lg - b|g|^{a} \, sign(g), \tag{29}$$

with $L > \ell$. This is designed to perform finite-time sliding mode convergence. To obtain the time of synchronization, consider the nonlinear sliding surface of (28). Substituting (22) and (29) in (28), the sliding surface and its time differential are respectively given by:

$$s = -(L - \ell) g, \tag{30}$$

and

$$\dot{s} = -(L - \ell)\left(s - \ell g - b|g|^{a} \, sign(g)\right). \tag{31}$$

Relying on equation (30),

$$|s|sign(s) = -(L-\ell)|g|sign(g) \tag{32}$$

Taking into account the fact that, p and m are odd,

$$s\dot{s} = -Ls^2 - b(L-\ell)^{(1-a)}|s|^{a+1}. \tag{33}$$

Consequently, with the Lyapunov function of (16), equation (33) can be rewritten as

$$\dot{V} = -2LV - b(L-\ell)^{(1-a)}2^{\frac{a+1}{2}}|V|^{\frac{a+1}{2}}. \tag{34}$$

The synchronization time can therefore be deduced as:

$$T(g_0) = \frac{1}{L(1-a)}\ln\left(1+\frac{L(2V(g_0))^{\frac{1-a}{2}}}{b(L-\ell)^{1-a}}\right). \tag{35}$$

The synchronization time is shorter when $\ell = 0$ than otherwise; thus the second order sliding mode becomes less accurate for this controller, when the sliding variable is used. Equation (35) enables first to assert that the controller achieves fast finite-time sliding mode according to the Lyapunov theorem whatever the choice of the nonlinear sliding surface is. Secondly, with the sliding equation, synchronization occurs for all state variables of errors' system in (11) and (22).

The curves on Figure 4 represent the numerical results of (7) obtained with the controller of (29) when the parameter values are $b = 5\cdot10^{-6}$, $a = \frac{1}{3}$ and $L = 2$. These curves (in blue on Figure 6) do not suffer from chattering, even at a precision of 10^{-15}; they are very closed to zero compared to the previous results.

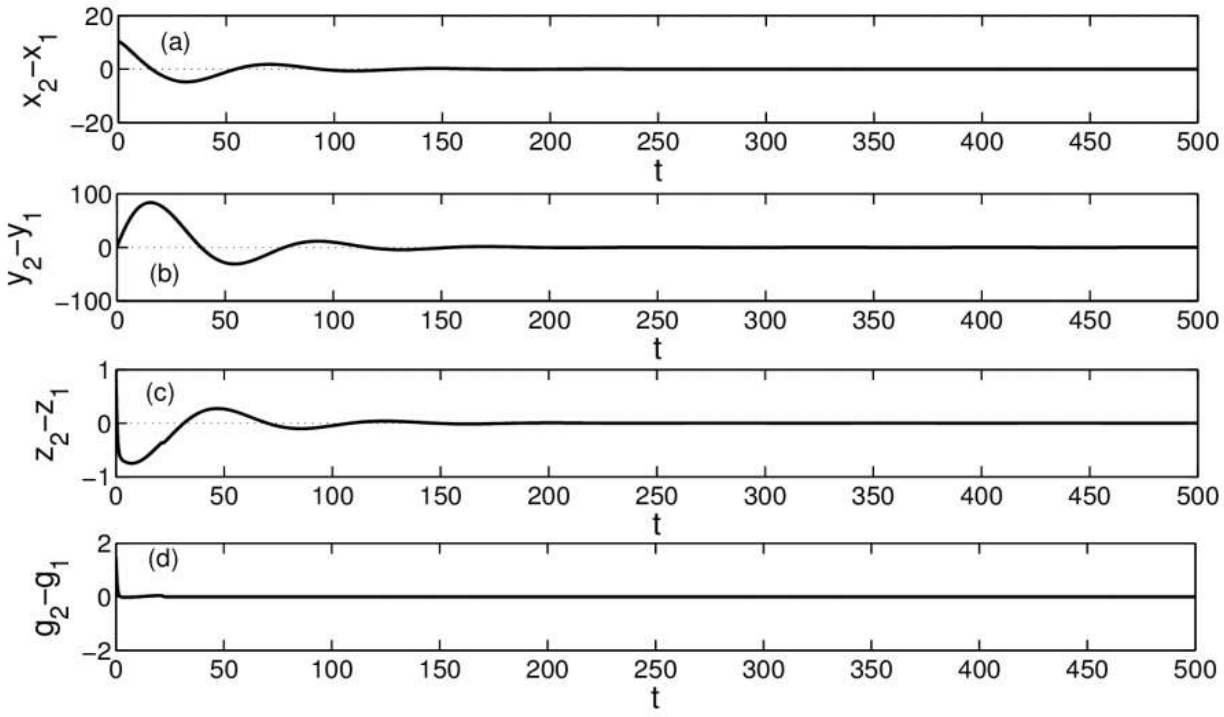

Figure 4: Synchronization error variable X versus dimensionless time t when the implicit variable g is used. a), b), c) and, d) present the time evolution of the errors on the variables x, y and, z as well as on the sliding variable g in the case of a nonlinear sliding surface.

In the present case, the control parameters k and L for SMC and TSM methods are respectively chosen to be equal. These parameters strongly influence the synchronization times which are moreover close to each other.

Comparing to the previous linear manifold approach, the TSM method in this section offers properties to the errors' system which can be recognized equivalent to those usually obtained when the FTSM method is applied. Thus, the nonlinear manifold solution enhances convergence speed and achieves finite-time convergence as already observed by [8]. In the following subsection, the nonlinear manifold elaborated so far will provide even more precision and easy implementation in PSpice.

Fast finite-time method: Simple approach with hyperbolic tangent manifold surface

It should be noted that the simplicity of the equation of the variable g makes it possible to choose the nonlinear controller of any form that one wishes, without having to worry about the challenging calculus of the usual approach. Thus, in the rest of the paper the focus will be on the experimental aspect and on the synchronization time. After considering several cases of nonlinearities, the most advantageous case was found to be the hyperbolic tangent (tanh). Far from being an advantage in practice, the hyperbolic tangent function provides the solution to the problems of the TSM using the simple approach. It is important to remember that in the preceding paragraph, it has been demonstrated that the nonlinear second order surface usually used is no longer efficient. With the hyperbolic tangent nonlinear surface, the properties of the FTSM are obtained as can be seen in Figure 6 (comparative color figures).

The difficulty with a usual nonlinear manifold surface is to realize in practice the found g^a function that guaranties the properties offered by FTSM method. In the present work, the found g^a is the cubic root function. According to [14], the cubic root has first been implemented in PSpice using the fuzzy logic approach. The output of our experiment was that this part of the controller helps rather to reduce the chattering phenomenon instead of eliminating it. Apart from that, the cubic root sub-circuit was not accurate when its input was worth less than the absolute value of 0.01 corresponding to its computational error. The direct effect of this disadvantage is that, the controller will not be efficient when the values of g tend to zero. To bypass that difficulty, the cubic root function be replaced by the hyperbolic tangent function. This later function which is known to be bounded by the root function can easily be realized in practice using the Op-Amp non-linearity at saturation [15].

Consequently, let's consider the new sliding surfaces and controller given respectively by equations (36) and (37):

$$s = \dot{g} + b\tanh(|g|)sign(g) = 0, \tag{36}$$

and

$$u = -\alpha f - \alpha AI_k - Lg - b\tanh(|g|)sign(g). \tag{37}$$

These equations are designed to perform fast finite-time sliding mode. Substituting (22) and (36) in (37), the sliding surface and its time derivative take the following forms respectively:

$$s = Lg, \tag{38}$$

$$\dot{s} = -L\dot{g}, \tag{39}$$

$$\dot{s} = -L(s - b\tanh(|g|)sign(g)). \quad (40)$$

According to (38),

$$|s|sign(s) = -L|g|sign(g). \quad (41)$$

Thus,

$$s\dot{s} = -Ls^2 - b|s|\tanh\left(\frac{|s|}{L}\right). \quad (42)$$

Taking into account the Lyapunov function (16), equation (42) becomes

$$\dot{V} = -2LV - b\sqrt{|2V|}\tanh\left(\frac{\sqrt{|2V|}}{L}\right) \quad (43)$$

which is similar to (45) for $V = \frac{2V}{L^2}$, $k = 2L$ and, $q = \frac{2b}{L}$.

The direct integration of (43) and (45) being rather complex, it can however be approximated to obtain the expression of the time at which the states' system converges to the equilibrium point.

Let's find a negative expression which can be bounded on both sides by the left-hand side of inequality (7) without the loss of convergence properties. In fact if $0<a<1$ then

$$\forall w \in R, -|w|^a \le -|\tanh(w)|. \quad (44)$$

This can be used to bound the following expression of the Lyapunov function derivative:

$$\dot{V} = -kV - q\sqrt{V}\tanh\left(\sqrt{V}\right). \quad (45)$$

Using equation (44) where w is replaced by $\sqrt{V}$, one side of equation (45) can be bounded as shown in inequality (46)

$$-kV - qV^{\frac{a+1}{2}} \le -kV - q\sqrt{V}\tanh\left(\sqrt{V}\right). \quad (46)$$

To bound the other side of equation (45), a real a and $(k',q')>(0,0)$ can be found that verify the following inequality:

$$-k'V - q'V^a \ge -kV - q\sqrt{V}\tanh\left(\sqrt{V}\right). \quad (47)$$

Applying the logarithm function on the inequality (47) leads to:

$$a - \frac{1}{2} \le \frac{-\ln(q') + \ln\left[K\sqrt{V} + q\tanh\left(\sqrt{V}\right)\right]}{\ln(V)}, \quad (48)$$

with $K = (k - k')$ and k' chosen to fulfill the condition $(k - k')>0$. If $w = \sqrt{V}$ then the inequality (44) leads to

$$\tanh\left(\sqrt{V}\right) \le \sqrt{V}. \quad (49)$$

Bounding (48) by using (49) gives the following relation:

$$a-\frac{1}{2}\le\frac{-\ln(q')+\ln\left[K\sqrt{V}+q\tanh\left(\sqrt{V}\right)\right]}{\ln(V)}\le\frac{-\ln(q')+\ln\left(K\sqrt{V}+q\sqrt{V}\right)}{\ln(V)}. \quad (50)$$

In the simplified form, equation (50) can be reduced to the following form:

$$a\le 1+\frac{-\ln(q')+\ln(K+q)}{\ln(V)}. \quad (51)$$

Using the particular solution $q'=(K+q)$ under the condition $a\le\frac{1}{2}$ allows verifying inequality (47). According to equation (8) the convergent time $T(g_0)$ of (45) is defined as:

$$T_1(g_0)\le T(g_0)\le T_2(g_0). \quad (52)$$

Here $T_1(g_0)$ and $T_2(g_0)$. are convergent time obtained from left-hand side of inequalities (46) and (47) respectively. The Lyapunov function derivative with a hyperbolic tangent expression as in (45) is mathematically proved to converge to zero within finite time which can be estimated by (52). The synchronization time is then given by (52) bounded again by (53) and (54) as follows, for $a\le\frac{1}{2}$:

$$T_1(g_0)=\frac{2}{k(1-a)}\ln\left(\frac{kV^{\frac{1-a}{2}}(g_0)+q}{q}\right), \quad (53)$$

$$T_2(g_0)=\frac{1}{k'(1-a)}\ln\left(\frac{k'V^{1-a}(g_0)+q'}{q'}\right). \quad (54)$$

|Figure 5 represents the plot of equation (43) obtained for FTSM method. It shows that the designed manifold surface enhances the exponential convergence of the error system which is an improvement compared to the previous surfaces.

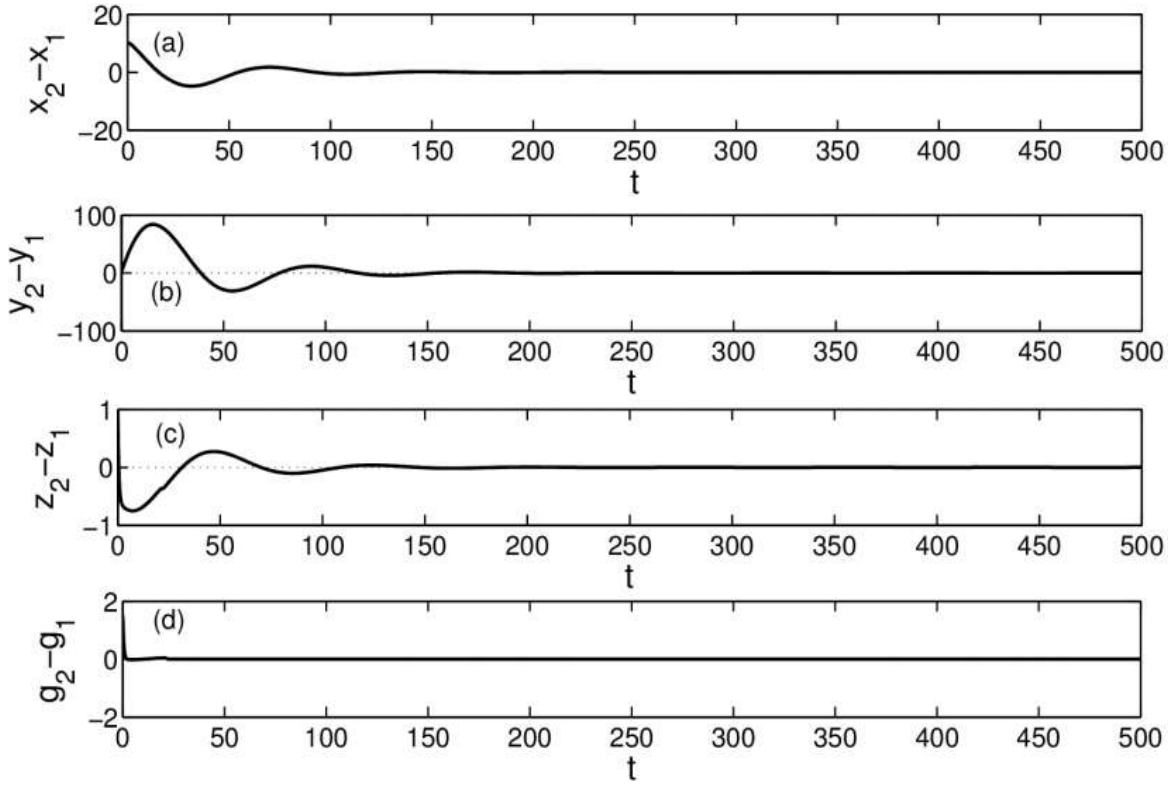

Figure 5: Synchronization of error variable X versus dimensionless time t when implicit variable g is used. a), b), c) and, d) present the result with hyperbolic tangent of sliding variable. Graphs from top to bottom show in each column, error on x, y and, z error variables and the sliding variable g.

The same result is confirmed by the black curves in Figure 6 of the numerical comparative results. In this case, the error variables do not suffer from the chattering phenomenon and the synchronization error is zero. A comparison of the three techniques (SMC, TSM and FTSM) is depicted by the whole Figure 6 where the closeness of synchronization error variable X to equilibrium point E is better achieved with the FTSM (curves in black color). This sustains that, with equation (43) the designed manifold surface enhances better the exponential convergence of the errors' system. It can also be noticed that the use of tangent hyperbolic function has completely eliminated the chattering phenomenon (black color curves).

PSpice results

Jerk circuits offer the possibility to access their states variables externally, and therefore, to control the system using anyone of its variables. The controller can also be introduced into the response circuit as current or/and voltage according to the choice of the user. In addition, voltages across the capacitors are accessible, enabling to build the sliding variable without

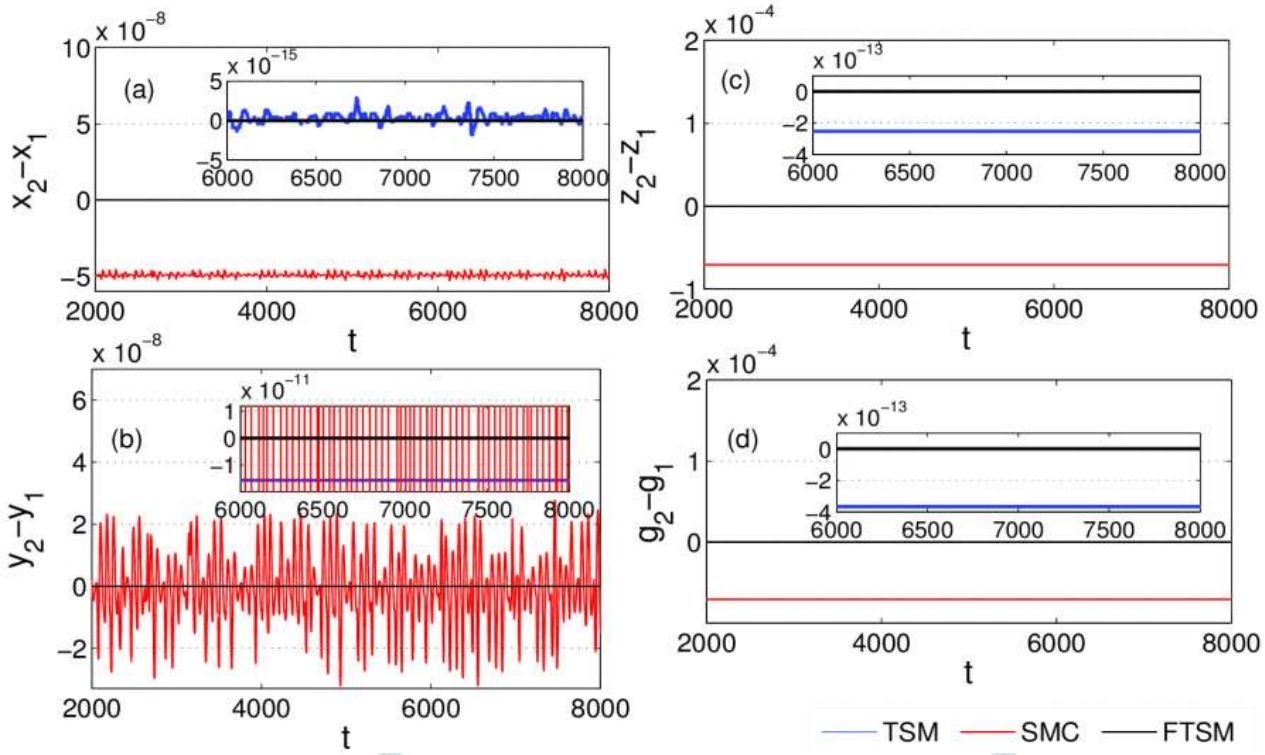

Figure 6: The closeness of synchronization error variable X to equilibrium point E. Red color is used for the result with linear sliding surface; Blue color presents the result with nonlinear sliding surface and black is reserved to the result with hyperbolic tangent of sliding variable. Graphs (a), (b), (c) and, (d) show error on x, y, z and g canals respectively.

introducing additional filters. For the FTSM method, the controller can be entirely built using the sliding variable, in the present case a voltage, while for TSM and SMC methods implying linear manifold surfaces, the nonlinear current is the necessary element to build the linear part of the controller on the response system itself.

The experimental realization of various techniques studied in the previous sections has been carried out using PSpice. In each circuit, the numbers referring the nodes (seen Figure 1) of master or slave are followed by m or s respectively. If between the node number and m or s a letter f appears, the signal correspond to the output of an ideal voltage control voltage source (is input been that node). The synchronization block diagram of SMC method depicted by Figure 7 confirms the use of the state's variables. Figure 8 reports the TSM method using sliding variables, and the hyperbolic tangent based FTSM is presented in Figure 9 Running the PSpice simulations (Figure 10), it can be noticed that each method implemented here converges to zero. It should be remarked that a very stark zooming of the experimental results enables to appreciate the gradual suppression of the chattering from one method to the next (Figure 11).

With the precision in Figure 11, the chattering phenomena that appeared in numerical results repeat itself for each method. For reasons of simplicity, we avoided building the sign block as for the TSM method in the synchronization circuit for the SMC method, contrary to Ref. [16]. Instead, a tiny part of nonlinear current (0.01) is tapped and reintroduced it into the JFET source node, which is simpler than the sign block for similar result. Notice that an increase in the value of the parameter q reduces the synchronization time, but

increases the chattering amplitude consequently; in other words, it decreases the robustness of the system [17].

In Figure 11, curves corresponding to SMC (a, b, c) and TSM (d, e, f, g) methods are plotted at precision of 10^{-6}. For FTSM method, the curves are plotted with precision of 10^{-8} for V_{C_1} while other states variables are kept at zero. The later method remains therefore the most precise one. Thus, the SMC method results present high chattering disturbance that goes diminishing with the TSM method, and disappears with the FTSM.

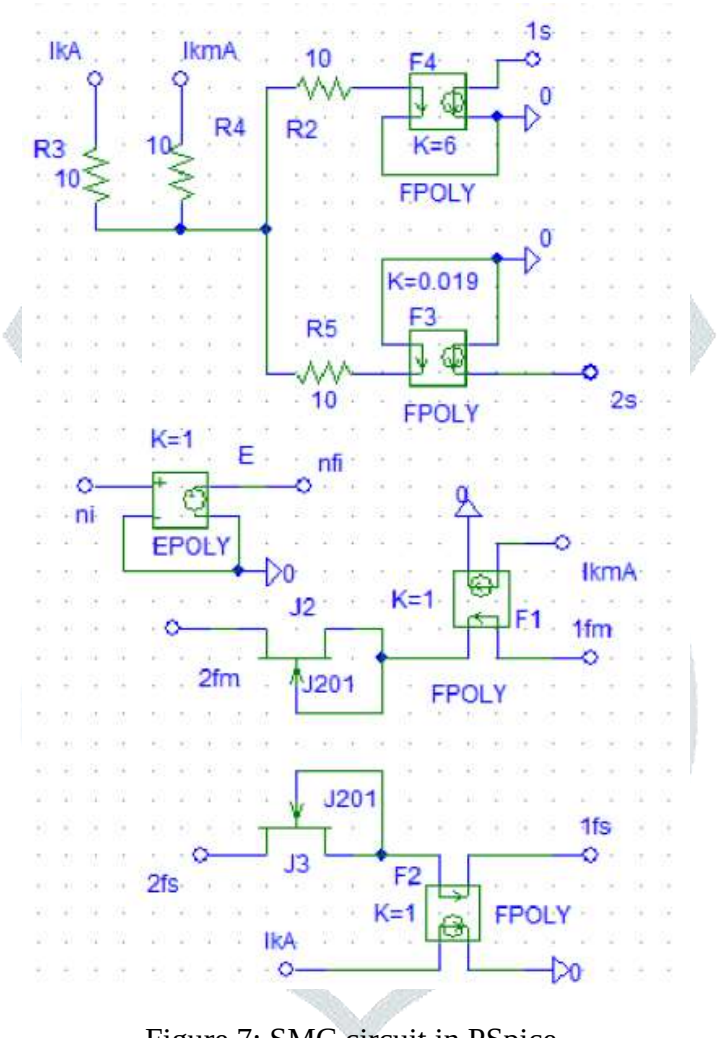

Figure 7: SMC circuit in PSpice.

As in Ref. [18], it is expected that the FTSM method will be the one with largest and more complicated topology in the PSpice implementation. Surprisingly, in the present work, that is not the case. Its topology has been found to be the simplest of the three methods (see Figure 7, Figure 8 and, Figure 9). In fact, the drive-response connection schemes both for the SMC and TSM methods (Figure 7, Figure 8) use field effect transistors to generate the nonlinear

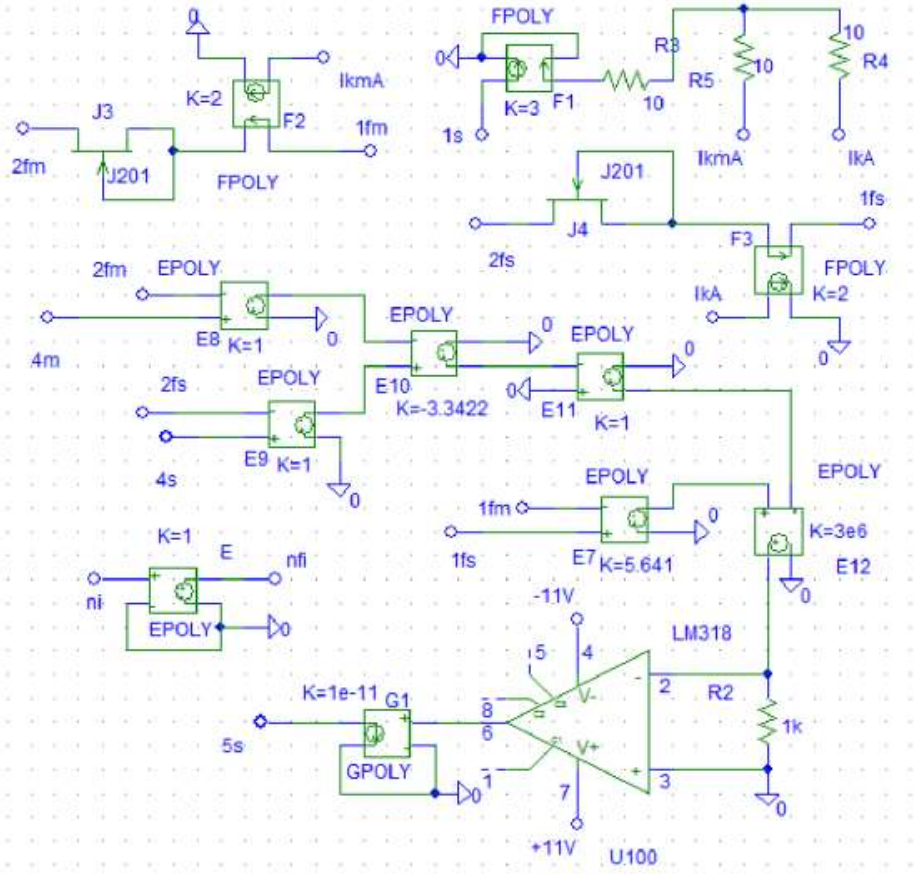

Figure 8: TSM circuit with sign function.

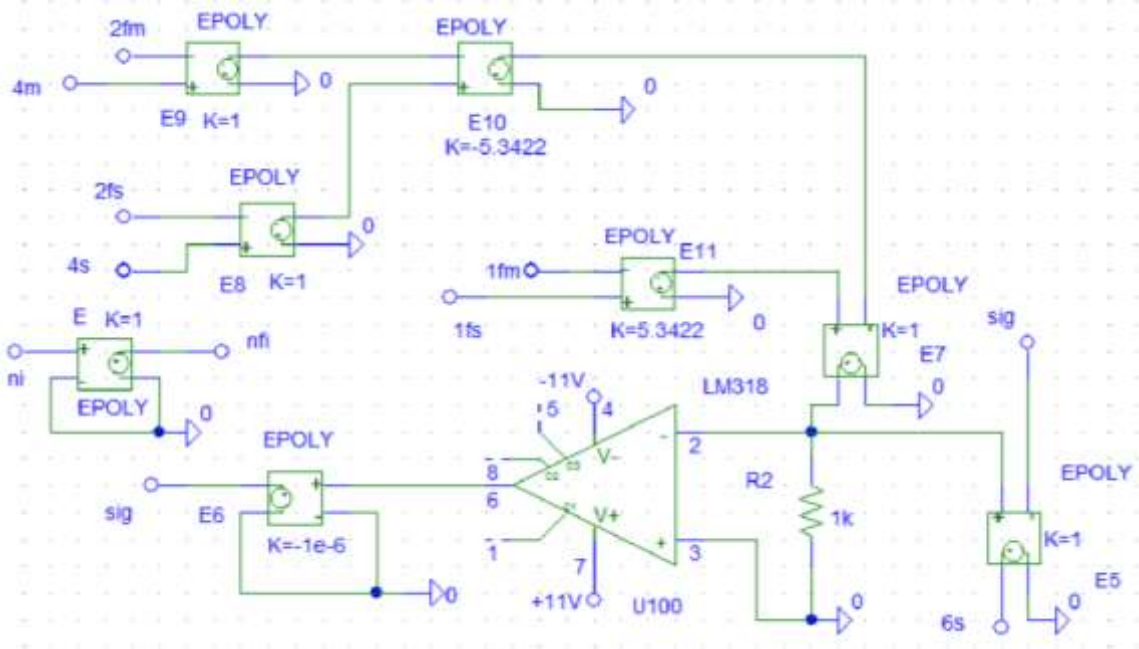

Figure 9: FTSM circuit in PSpice using no filter. The circuit presents the advantage of being simpler, compared to the circuits related to SCM (Figure 7) and TSM (Figure 8) respectively.

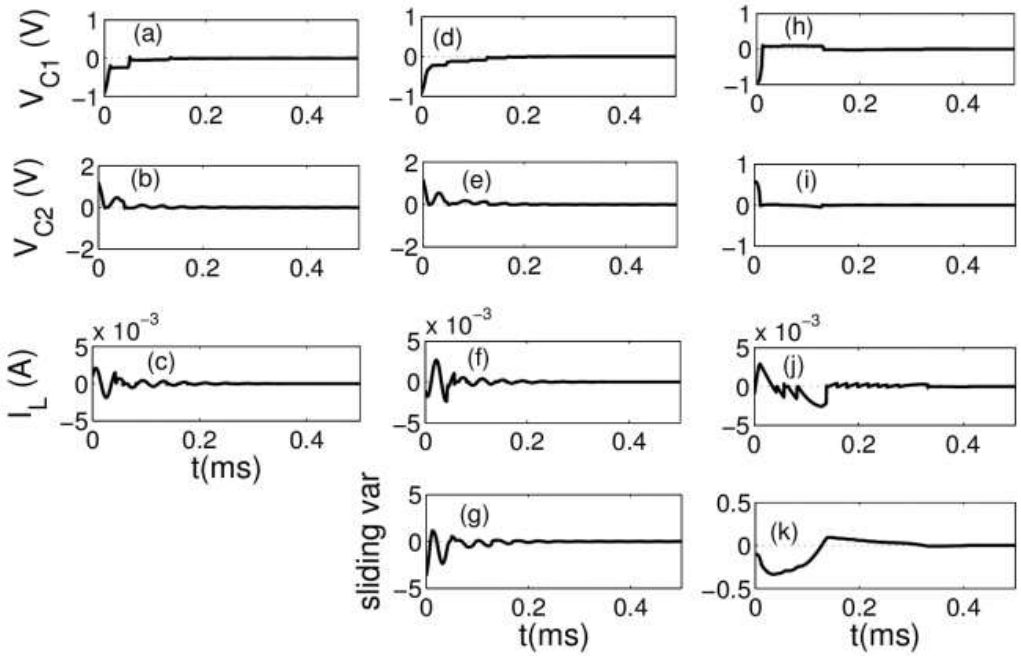

Figure 10: PSpice synchronization error variables versus t. The first column presents the result of the SCM method; the second column corresponds to the result of TSM method when the sliding variable and linear surface are used. The right column expresses the result with hyperbolic tangent of sliding variable (FTSM method). Graphs from top to bottom show in each column errors on V_{C_1}, V_{C_2}, I_L and, g canals respectively.

controller current, which is not the case for the FTSM method (Figure 9). Since the chattering is a high frequency phenomenon, the field effect transistors can get into non desired dynamics [17], [19] and affect the synchronization of those systems. In addition, the current controlled voltage sources and the voltage controlled current source present in for the SMC and TSM methods are not as easy to be implemented in truth laboratory experiment, because they exist in PSpice just for simulation purpose. Thus, in the present work, the FTSM method topology involving only voltage controlled voltage source is the one that can be easily realized experimentally, as such sources can be replaced by Op-Amp and resistors.

For all the three methods, the nominal values of components used in the PSpice simulations were same for the drive and the response circuits, namely: $C_1 = 10nF$; $C_2 = 47.4nF$; $L = 0.8mH$ and $R = 10\Omega$. The initial conditions were also the same for all the methods and chosen far enough from each other to test the robustness of the FTSM method with respect to the equilibrium point. They were worth $I_{C_1} = 0.07$; $I_{C_2} = 0.07$ and $I_L = 8 \cdot 10^{-6}$ for the drive circuit, and $I_{C_1} = 1$; $I_{C_2} = 2 \cdot 10^{-4}$ and $I_L = -1 \cdot 10^{-3}$ for the response one respectively. The results of PSpice simulation are plotted using MatLab environment.

Definitely, the FTSM method involving the hyperbolic tangent in its manifold surface gives the best results (Figure 11) and has the simplest topology which is in addition easier to be realized experimentally (Figure 9).

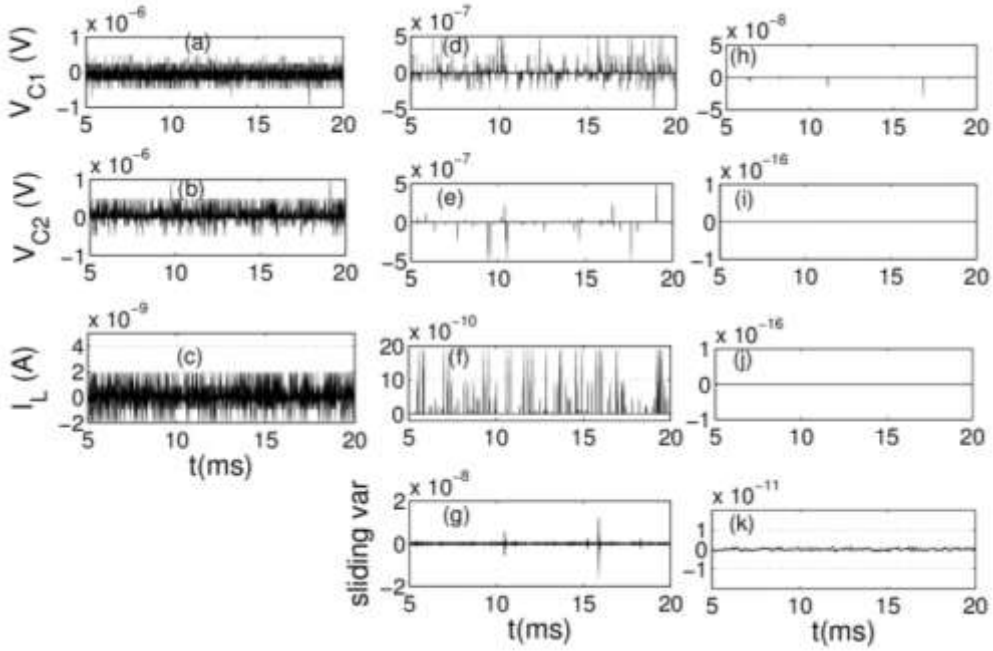

Figure 11: Chattering behavior in Synchronization error variables versus t zooming. The first column depicts the result of the SCM method; the second column corresponds to the result of TSM method when sliding variable and linear surface are used. The right column expresses the result with hyperbolic tangent of sliding variable (FTSM method). Graphs from top to bottom show in each column errors on V_{C_1}, V_{C_2}, I_L and, g canals respectively. The precision increases from the left to right column.

Definitely, the FTSM method involving the hyperbolic tangent in its manifold surface gives the best results (Figure 11) and has the simplest topology which is in addition easier to be realized experimentally (Figure 9).

Conclusions

The aim of this paper was to design and realize both numerically and analogically a fast terminal sliding mode controller for the synchronization of two single Op-Amp-based jerk circuits. It was observed that the sliding variable obtained from the jerk form equation makes the calculus easier as well as the PSpice realization. Furthermore, all sliding control methods applied on the errors' system provided finite-time stability according to the Lyapunov theorem when the sliding equation is used. The results obtained from different sliding mode control methods show that, the hyperbolic tangent nonlinear manifold surface provides exponential convergence and fast terminal sliding mode stability to the errors' system whatever initial conditions were chosen.

References

[1] T. Venkataraman and S. Gulati. “Terminal slidingmodes: A new approach”. 5th Int. Conf. Advanced Robotics, vol. 1, 443–448, 1991.

[2] S. Yu and Z. Man. “Fast terminal sliding-mode control design for nonlinear dynamical systems”. IEEE Trans. Circuits Syst I:Fundamental Theory and Applications, vol. 49, no. 2, 261–264, 2002.

[3] S. Vaidyanathan and S. Sampath. “Anti-synchronization of the hyper chaotic, lorenz systems by sliding mode control”. IJCSE, vol. 3, no. 6, 2450–2457, Jun. 2011.

[4] S. Song, X. Zhang, and Z. Tan. “Rbf neural network based sliding mode control of a lower limb exoskeleton suit”. Strojniˇ ski vestnik-Journal of Mechanical Engineering, vol. 60, no. 6, 437–446, Jan. 2014.

[5] B. Shtessel, A. Shkolnikov, and D. Brown. “An asymptotic second-order smooth sliding mode control”. Asian J. Control, vol. 5, no. 4, 498–504, Dec. 2003.

[6] P. Tiwari, S. Janardhanan, and M. Nabi. “A finite-time convergent continuous time sliding mode controller for spacecraft attitude control”. 11th Int. Workshop VSS, pages 399–403, Jun. 2010.

[7] C. Suttirak and C. Pukdeboonn. “Finite-time convergent sliding mode controller for robot manipulator”. Applied Mathematical Sciences, vol. 7, no. 63, 3141–3154, 2013-.

[8] G. Jie, S. Yongzhi, and L. Xiangdong. “Finite-time sliding mode control a reentry vehicle with blended aerodynamic surfaces and a reaction control system”. CJA, vol. 27, no. 4, 964–976, Nov. 2014.

[9] J. Li and L. Yang. “Finite-time terminal sliding mode tracking control for piezoelectric actuators”. Hindawi Publishing Corporation Abstract and Applied Analysis Volume, pages null–9, Mar. 2014.

[10] A. Benamor, L. Chrifialaui, and M. Chaabane. “Sliding mode control, with integrator, for a class of mimo nonlinear systems”. Engineering, 2011. May.

[11] B. Shtessel, C. Edwards, L. Fridman, and A. Levant. “Sliding mode control and observation in control engineering.”. New York: Springer Science and Business Media, pages 1–42, 2013.

[12] R. Tchitnga, T. Nguazon, F. Louodop, and J. Gallas. “Chaos in a single op-amp–based jerk circuit: experi-ments and simulations”. IEEE Trans. Circuits Syst. II: Exp. Briefs, vol. 63, no. 3, 239–243, Mar. 2016.

[13] A. Rhif. “A high order sliding mode control with pid sliding surface: simulation on a torpedo”. IJITCA, vol. 2, no. 1, 1–13, Jan. 2012.

[14] J. Slezak and J. Petrozela. “Evolutionary synthesis of cube root computational circuit using graph hybrid estimation of distribution algorithm”. Adio engineering, vol. 23, no. 1, 549–558, Apr. 2014.

[15] R. Tchitnga, R. Z. Nanfa’a, F. Pelap, P. Louodop, and P. Woafo. “A novel high-frequency interpretation of a general purpose op-amp-based negative resistance for chaotic vibrations in a simple a priori non chaotic circuit”. J. Vib. Control, pages 1–8, May. 2015.

[16] J. Sprott. “Simple chaotic systems and circuits”. Am. J. Phys., vol. 8, no. 68, 758–763, Nov. 2000.

[17] R. Tchitnga, H. Fotsin, B. Nana, F. P. Louodop, and P. Woafo. “Hartley’s oscillator: the simplest chaotic two-component circuit”. Chaos Solitons Fract, vol. 45, 306–313, Dec. 2012.

[18] H. Brandtst¨ adter. “Sliding mode control of electromechanical systems”, 2014. Ph.D. thesis, Lehrstuhl für Steuerungs- und Regelungstechnik, Technische Universit¨ at M ¨ unchen, M ¨ unchen, Germany; 2014.

[19] S. H.-L. Tu and Y.-H. Cheng. “Realization of fractional-order capacitors with field-effect transistors”. Inter-national Scholarly and Scientific Research and -Innovation, vol. 6, no. 11, 562–565, Nov. 2012.